IOP Publishing Physical Biology
Phys. Biol. **11** (2014) 000000 (11pp) UNCORRECTED PROOF

Buffer regulation of calcium puff sequences

Daniel Fraiman[1,3] **and Silvina Ponce Dawson**[2]

[1] Laboratorio de Investigación en Neurociencia, Departamento de Matemática y Ciencias, Universidad de San Andrés, (1644) Buenos Aires, Argentina
[2] Departamento de Física, FCEN-UBA, Ciudad Universitaria, Pabellón I, (1428) Buenos Aires, Argentina

E-mail: dfraiman@udesa.edu.ar and silvina@df.uba.ar

Received 15 August 2013, revised 20 December 2013
Accepted for publication 20 December 2013
Published DD MM 2014

Abstract

Puffs are localized Ca^{2+} signals that arise in oocytes in response to inositol 1,4,5-trisphosphate (IP_3). They are the result of the liberation of Ca^{2+} from the endoplasmic reticulum through the coordinated opening of IP_3 receptor/channels clustered at a functional release site. The presence of buffers that trap Ca^{2+} provides a mechanism that enriches the spatio-temporal dynamics of cytosolic calcium. The expression of different types of buffers along the cell's life provides a tool with which Ca^{2+} signals and their responses can be modulated. In this paper we extend the stochastic model of a cluster of IP_3R-Ca^{2+}channels introduced previously to elucidate the effect of buffers on sequences of puffs at the same release site. We obtain analytically the probability laws of the interpuff time and of the number of channels that participate of the puffs. Furthermore, we show that under typical experimental conditions the effect of buffers can be accounted for in terms of a simple inhibiting function. Hence, exploring different inhibiting functions we are able to study the effect of a variety of buffers on the puff size and interpuff time distributions. We find the somewhat counter-intuitive result that the addition of a fast Ca^{2+} buffer can increase the average number of channels that participate of a puff.

Keywords: calcium dynamics, puffs sequences, buffers, EGTA, BAPTA

1. Introduction

Calcium (Ca^{2+}) signals are ubiquitous across cell types [1]. Changes in the cytosolic Ca^{2+} concentration lead to a variety of end responses that include muscle contraction, neuronal communication, egg fertilization and cell death. In spite of this ubiquity, Ca^{2+} signals are highly specific. This is possible because the responses not only depend on other cell components, but also on the spatio-temporal dynamics of the cytosolic Ca^{2+} concentration itself [2]. Ca^{2+} signals always involve Ca^{2+} entry through specialized channels that are located on the plasma membrane or on the membrane of internal stores, like the endoplasmic reticulum. Given that prolonged high elevations of $[Ca^{2+}]$ give rise to cell death, cells need to control $[Ca^{2+}]$ very tightly. Among others, the presence of *buffers* (usually, large proteins) that trap Ca^{2+} provides a mechanism by which the content of free Ca^{2+} in the cytosol can be quickly decreased upon Ca^{2+} entry. But buffers not only decrease $[Ca^{2+}]$ uniformly, they also alter the spatio-temporal dynamics of $[Ca^{2+}]$ [3, 4]. Thus, the expression of different types of buffers along the cell's life provides a tool with which Ca^{2+} signals and their responses can be modulated.

The spatio-temporal properties of intracellular Ca^{2+} signals have been extensively characterized in *Xenopus laevis* oocytes using optical techniques [5]. In these cells, the signals arise upon the liberation of Ca^{2+} from the endoplasmic reticulum into the cytosol through IP_3 receptors (IP_3Rs) which are Ca^{2+} channels. These studies have revealed a hierarchical organization of release events which is consistent with the IP_3Rs being organized in clusters of tens of channels with a typical inter-cluster distance of a few micrometers. In this way, the smallest release events ('blips') can be associated to Ca^{2+} liberation through single IP_3Rs, Ca^{2+} 'puffs' correspond to the concerted opening of several IP_3Rs within a cluster and global waves involve cluster–cluster interactions via Ca^{2+}-induced Ca^{2+} release (CICR) [6]. Thus, 'puffs' constitute ubiquitous 'elementary events' of intracellular Ca^{2+} signaling, which can both have local signaling functions in their own right, and serve as building blocks from which global signals are constructed.

[3] Author to whom any correspondence should be addressed.

Different approaches have been proposed to describe Ca^{2+} release through clustered IP_3Rs depending on the spatial and time scale that are tried to be resolved. The 'fire-diffuse-fire' (fdf) model, for example, which was introduced to study $[Ca^{2+}]$ waves, simplified clusters by considering them as discrete excitable Ca^{2+} release units that opened when a certain threshold level of Ca^{2+} was reached [7, 8]. A stochastic version of the fdf model was introduced in [9, 10] by assuming that the threshold was a random variable. More recently, we developed a phenomenological stochastic model of a cluster based on observed puff properties which we included in a more realistic stochastic fdf model [11]. Fdf-like models do not take the internal structure of the clusters into account. Some models that do describe the individual openings of IP_3Rs in a cluster simplify their descriptions by considering that $[Ca^{2+}]$ is homogeneous throughout the cluster [12–19]. Models that include spatial inhomogeneities inside the cluster are computationally expensive if the same resolution is used inside and outside the cluster [20–22]. Other models use different spatial grids depending on the region that is described [22, 23].

These previous modeling attempts show that having a simple effective IP_3R-cluster model that is able to reproduce observed puff properties is a good choice if one is not interested in describing the intracluster dynamics in detail. Several questions arise regarding this issue. First, whether it is possible to model the cluster's response as a whole without describing the dynamics of each individual IP_3R and without knowing the spatio-temporal distribution of Ca^{2+} and of the buffers that interact with it within the cluster region. Second, to what extent an effective model that is able to reproduce the observations obtained under certain experimental conditions can still describe the cluster dynamics in other settings. In this paper we address this last issue. More specifically, we analyze how the presence of different amounts and types of buffers modulate the response of the cluster. The way in which buffers affect the dynamics of isolated or clustered IP_3Rs has been studied in various papers [24–26]. In particular, these studies show that the presence of an immobile buffer decreases the mean open time and increases the mean closed time of single IP_3Rs while mobile buffers do not affect the release kinetics in this case. In the case of clustered IP_3Rs, however, the mean time during which there is Ca^{2+} release can increase or decrease in the presence of a fast (mobile) buffer. It increases if the buffer moderates the inhibiting effect of high Ca^{2+} concentrations on IP_3Rs. In particular, this is the case for clusters where IP_3Rs are closely packed. According to these modeling studies, the mean Ca^{2+} release duration decreases when the net effect of the buffer is to decrease Ca^{2+} coupling via CICR. This occurs when the typical mean separation between IP_3Rs is large enough. These conclusions agree with other studies that show that the intracluster spatial organization plays a relevant role on the emergent behavior of the cluster as a whole [27–29]. Since IP_3Rs become open upon IP_3 and Ca^{2+} binding, changes in the IP_3 concentration change the mean distance between activatable IP_3Rs. Disrupting CICR with the presence of buffers, on the other hand, changes the mean distance over which an open IP_3R can exert an effect. Thus, both changing the $[IP_3]$ or the buffer concentrations have a similar effect to altering the intracluster spatial organization and, thus, the cluster release dynamics [27, 29, 30].

In this paper we extend the simple IP_3R-cluster model introduced in [33] to take into account the effect of buffers on the dynamics of sequences of puffs that occur at one release site. More specifically, we look at how the number of channels that participate of each puff (the *puff size*) and the interpuff time interval vary in the presence of different types of buffers. The key quantity with which we model the effect of the buffers is the inhibition probability of the IP_3Rs that participate of a Ca^{2+} release event. The relevance of the inhibitory effects on sequences of Ca^{2+} signals has been pointed out in a series of papers that deal with the dynamics of global signals (spikes) that involve the CICR from several IP_3R clusters [31, 32]. In particular, these studies have shown that the interspike time, T, is a random variable whose standard deviation, σ_T, is linearly related to the mean, $\langle T \rangle$, with a slope that depends on a global negative feedback [31]. In this setting, however, it is unknown what this global mechanism could be and, in principle, could be different from the processes included in the model considered in the present paper (e.g., some global mechanism mediated by the dynamics of luminal Ca^{2+}. In our problem we assume that the inhibition probability is an increasing function of the number of open channels. Due to the simplicity of the model, the probability distributions of puff size and interpuff times can be obtained analytically. Furthermore, very general conclusions can be drawn on the model's behavior in terms of some basic features of the inhibiting function. In particular, we find the somewhat counter-intuitive result that the addition of a fast Ca^{2+} buffer can amplify puff sizes and decrease the interpuff time. The study of the dynamics of (global) Ca^{2+} spikes has important implications for understanding the ways in which cells decode external stimuli. Although we do not look at this global dynamics as done in [31, 32], the behavior of our model can be used to understand certain features of the observations with implication for the robustness of the Ca^{2+} signaling mechanisms [31].

2. Results

2.1. A simple IP_3R-cluster model

Modeling the behavior of an IP_3R cluster as a whole is not straightforward since the individual IP_3Rs do not act independently of one another: Ca^{2+}, the ion that flows when the channels open, also modulates the open probability of the individual receptors. On the other hand, Ca^{2+} exerts a 'dual' effect. While Ca^{2+} binding to certain sites of the IP_3R induces channel opening (provided that IP_3 is also bound to the IP_3R), its binding to other sites of lower affinity induces channel closing. For this reason, the IP_3R open probability, P_o, increases with increasing $[Ca^{2+}]$ for small values of $[Ca^{2+}]$ and decreases for large values. It can be assumed that $[IP_3]$ remains constant during the time course of the experiments done in oocytes in which Ca^{2+} puffs and waves are elicited. For these experiments, at the cytosolic basal values of $[Ca^{2+}]$ ($\sim$40 nM), P_o is an increasing function of $[Ca^{2+}]$. It may also

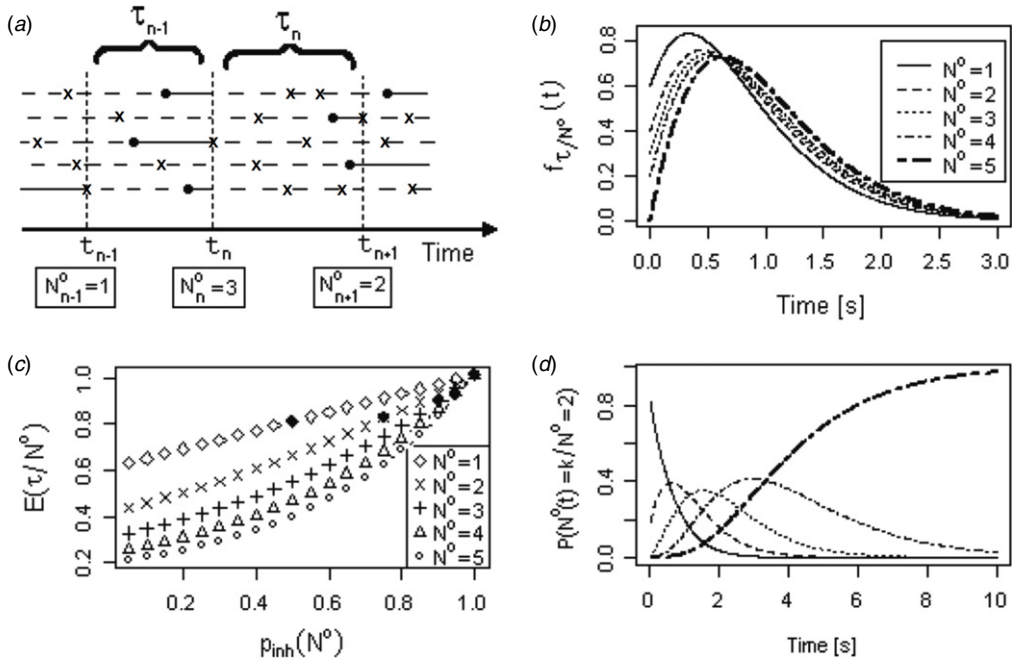

Figure 1. Model of cluster dynamics in terms of individual IP_3Rs presented in [33]. (*a*) Scheme of the model (see the text for more details). (*b*) Interpuff time conditional density, $f_{\tau_n/N_n^o}(t)$, for various values of various values of the number of open channels at the previous event, N_n^o. (*c*) Conditional expectation of the Interpuff time given N_n^o as a function of the inhibition probability. Filled black points correspond to the expected values of the densities shown in (*b*). (*d*) Probability that $N_{n+1}^o = k$ channels open during the $n+1$th event given that $N_n^o = 2$ channels opened during the nth puff, as a function of the time elapsed between both puffs, τ_n, for different values of k. In (*b*)–(*d*) it is $N = 5$, $\lambda_1 = 0.5\text{s}^{-1}$, $\lambda_2 = 1\text{s}^{-1}$, and $p_{\text{inh}}(1, 2, 3, 4, 5) = 0.5, 0.75, 0.9, 0.95, 1$.

be assumed that it is decreasing for the values of $[Ca^{2+}]$ that are attained within a cluster during a puff ($\sim$50 μM) [35]. In order to understand how channel–channel interactions affect the cluster's behavior, in a previous work [33] we studied the properties of sequences of 'puffs' that occurred at the same Ca^{2+} release site (i.e., cluster) in *Xenopus* oocytes. In particular, we analyzed the statistical properties of the sequences of puff amplitudes, A, and interpuff times, τ. Here by puff amplitude we mean the increment in fluorescence observed during the event. For a given experiment, A is an increasing function of the number of IP_3Rs that become open during the puff, N_o, and there is no need to distinguish between N_o and A. When comparing experiments performed with different amounts of dye or with exogenous buffers added the difference between N_o and A becomes relevant. This is particularly important in experiments in which fast buffers are added since they can compete with the Ca^{2+} dye for Ca^{2+} decreasing the observed fluorescence. In order to distinguish between N_o and A we will call them puff size and puff amplitude, respectively. In [33] we showed that, on average, large amplitudes, A_n, gave rise to large interpuff times, τ_n, and that small interpuff times, τ_n, were followed by puffs of small amplitude, A_{n+1}. We attributed these behaviors to the 'inhibitory' effect that Ca^{2+} exerts on IP_3Rs for the large values of $[Ca^{2+}]$ that are locally attained during a release event. Although, according to numerical estimates, $[Ca^{2+}]$ within the cluster goes back to its basal level very soon ($\sim$30 ms) after a puff ends [36], the dependence between A_n, and the subsequent interpuff time, τ_n is consistent with the individual IP_3Rs remaining inhibited for very long times ($\sim$2 s) compared to typical puff durations ($\sim$100 ms) [33]. The statistics of the experimental observations can be reproduced with the simple cluster model introduced in [33] which we analyze in detail in the current paper. In the model there are N identical IP_3Rs with IP_3 bound at any given time. The underlying assumption here is that the processes of IP_3 binding and unbinding are in equilibrium with one another so that there is a fixed fraction of IP_3Rs in the cluster with IP_3 bound. This is reasonable given that the kinetics of these processes is very fast. In the model we further assume that the channels can be in two closed states: inhibited or not. When all channels are closed, an uninhibited channel can open with a constant probability per unit time, λ_1, which is related to the probability that a Ca^{2+} ion binds to the activating site of the receptor at the basal $[Ca^{2+}]$. When one channel of the cluster opens, all other uninhibited channels of the cluster open too. Since the interpuff time is much larger than the puff duration, we neglect the time during which channels remain open in the model. Channels that open during the puff can go to the inhibited state with probability $p_{\text{inh}}(N^o)$, where N^o is the total number of channels that opened during the event. p_{inh} is a rather arbitrary increasing function of N^o that must satisfy $p_{\text{inh}}(N^o = 0) = 0$. In the model, inhibition only occurs during the puff (while $[Ca^{2+}]$ at the release site is large enough). An inhibited channel becomes uninhibited with probability per unit time, λ_2. The model is schematically depicted in figure 1(*a*). In this example there is a total of five IP_3-bound IP_3Rs, each of them represented by a horizontal line. The receptors can be inhibited (indicated with long dashed lines) or activatable (solid lines). The transition from the inhibited to the activatable or uninhibited state occurs

spontaneously with probability per unit time λ_2 (indicated with a solid circle in the figure). Random arrivals of Ca^{2+}ions to the close vicinity of each IP_3R (marked with crosses) occur with probability per unit time λ_1. If the Ca^{2+} ion arrives at the vicinity of an inhibited IP_3R, nothing happens. If, instead, the corresponding receptor is uninhibited, the arrival results in Ca^{2+}binding to an activating site of the channel, its subsequent opening and the opening of all other activatable channels of the cluster generating a puff (indicated with vertical dashed lines). During each puff, some of the uninhibited channels become inhibited with a probability that is an increasing function of the puff amplitude ($p_{\rm inh}(N^o)$). We neglect the duration of the puff, so that this inhibition occurs instantaneously upon the occurrence of the event. There are three puffs in the example of the figure involving the opening of one, three and two channels and the subsequent inhibition of one, three and one IP_3Rs, respectively.

Model and experiments can be compared assuming that the puff amplitude, A, is an increasing function of the number of channels that opened during the event, N^o (i.e. of puff size). The parameters, λ_2 and λ_1 were estimated for the experimental conditions of [33] by fitting some of the observations as explained in that paper. In the present paper we explore the behavior of the model for different choices of the inhibitory probability, $p_{\rm inh}(N^o)$. In particular, we determine how the puff size and the interpuff time distributions can change depending on very basic features of $p_{\rm inh}(N^o)$.

2.2. Analytic calculation of puff size and interpuff time distributions

The model captures the essence of puffs dynamics, in fact it predicts well [33] the number of IP_3Rs in a cluster [37] and is simple enough so that the relevant probability distributions can be computed in an analytic way as we show in this subsection. Given that there are N IP_3Rs with IP_3 bound at any given time in the cluster (i.e., there are N activatable IP_3Rs) and that all active IP_3-bound IP_3Rs (i.e., that are not inhibited) become open as soon as any one of them opens up, having N_n^o channels that open during the nth puff is equivalent to having $N-N_n^o$ inhibited channels in the cluster. Taking this feature into account it is possible to show that the conditional distribution of the nth interpuff time, τ_n, given that N_n^o channels opened during the previous puff, $F_{\tau_n/N_n^o}(t) \equiv P(\tau_n < t/N_n^o)$, is given by

$$F_{\tau_n/N_n^o}(t) = 1 - \overline{F}_{io}(t)^N \left(p_{\rm inh}\left(N_n^o\right) + \left(1 - p_{\rm inh}\left(N_n^o\right)\right) \frac{\overline{F}_{uo}(t)}{\overline{F}_{io}(t)} \right)^{N_n^o}, \quad (1)$$

where $\overline{F}_{uo}(t)$ ($\overline{F}_{io}(t)$) is the probability that a channel that was uninhibited (inhibited) immediately after the nth puff ended does not open before a time t has elapsed since the (nth) puff occurred. Thus, $\overline{F}_{uo}(t) = \mathrm{e}^{-\lambda_1 t}$, and

$$\overline{F}_{io}(t) = \begin{cases} \dfrac{\lambda_2 \mathrm{e}^{-\lambda_1 t} - \lambda_1 \mathrm{e}^{-\lambda_2 t}}{\lambda_2 - \lambda_1} & \text{if} \quad \lambda_1 \neq \lambda_2 \\ (1 + \lambda_1 t)\, \mathrm{e}^{-\lambda_1 t} & \text{if} \quad \lambda_1 = \lambda_2. \end{cases} \quad (2)$$

Figure 1(b) shows an example of the conditional interpuff time density, $f_{\tau_n/N_n^o}(t) = \frac{\partial F_{\tau_n/N_n^o}(t)}{\partial t}$ for various values of N_n^o and for a particular choice of $p_{\rm inh}$ (see figure caption). We observe that, by increasing N_n^o, the density moves to the right and its corresponding expected value increases. This means that, in this example, a large puff size (i.e., with large N_n^o) is followed by a large (on average) interpuff time. This behavior agrees with the experimental observations of [33]. However, this is not the only possible behavior allowed by the model: depending on how fast $p_{\rm inh}(N^o)$ increases with N^o the resulting conditional probability can behave differently. With our model we can explore a variety of scenarios since it is amenable to some analytic computations. In particular, equations (1)–(2) imply that the conditional expected value of the interpuff time, $E(\tau/N^o)$, is a function of N^o and of $p_{\rm inh}(N^o)$. We can then choose pairs of values, (N^o, $p_{\rm inh}(N^o)$), that satisfy $1 \leqslant N^o \leqslant N$, $0 \leqslant p_{\rm inh} \leqslant 1$, compute $E(\tau/N^o)$, and in this way explore the behavior of the model for different choices of $p_{\rm inh}(N^o)$. We show in figure 1(c) the plot of $E(\tau/N^o)$ as a function of some pair of values, (N^o, $p_{\rm inh}(N^o)$), in particular those that correspond to the particular choice, $p_{\rm inh}(N^o)$, with which we made figure 1(b) (solid symbols in figure 1(c)). We can observe in figure 1(c) that, if the inhibition probability does not depend on the number of channels (i.e., if $p_{\rm inh}(N_n^o) = $ constant), the conditional expected time, $E(\tau/N_n^o)$, decreases with N_n^o. This behavior is different from the one obtained in the example of figure 1(b). In the next section we discuss in detail some more realistic biophysical scenarios for $p_{\rm inh}(N_n^o)$ and study its consequences on the dynamics of puffs.

In order to determine the probability that N^o channels open during a puff, we define $N^{\rm act}(t)$ as the number of uninhibited (activatable) channels in the cluster after a time, t, elapsed since the last event occurred. Similarly, we define $N^o(t)$ as the number of channels that open during an event that occurs a time t after the previous one. $N^o(t)$ takes values between 1 and N and $N^{\rm act}(t)$ between 0 and N. $N^{\rm act}(t)$ and $N^o(t)$ are very similar: if a puff occurs a time, τ, after the previous one, then $N^{\rm act}(t = \tau) = N^o(t = \tau)$. The probability of having k uninhibited channels at time t, given that at $t = 0$ there was a puff with N^o open channels (and no other event occurred between 0 and t) is given by

$$P(N^{\rm act}(t) = k/N^o) = (\mathrm{e}^{\lambda_2 t})^{N-k} (1 - \mathrm{e}^{\lambda_2 t})^{k-N^o} (1 - p_{\rm inh}(N^o))^{N^o} \times \sum_{j=\max\{0, N^o-k\}}^{N^o} \binom{N^o}{j} \binom{N-N^o+j}{N-k} \left(\frac{p_{\rm inh}(N^o)(1 - \mathrm{e}^{-\lambda_2 t})}{1 - p_{\rm inh}(N^o)} \right)^j. \quad (3)$$

The probability that j channels open during the $n+1$th event that occurs a time, τ_n, after the nth one, given that there were N_n^o open channels during that previous event, is given by

$$P\left(N_{n+1}^o(\tau_n) = j/N_n^o\right) = \frac{P\left(N^{\rm act}(\tau_n) = j/N_n^o\right)}{1 - P\left(N^{\rm act}(\tau_n) = 0/N_n^o\right)}. \quad (4)$$

We show in figure 1(d) the conditional probability, $P(N_{n+1}^o(\tau_n) = j/N_n^o = 2)$ as a function of the interpuff time, τ_n, for the same parameters as in figure 1(b). We can observe that, for small interpuff times, $\tau_n < 0.5$ s, most likely, only one channel will contribute to the following event, while for

longer times ($\tau_n \geqslant 8$ s), most probably all N channels in the cluster will participate. At times of the order of 8 s all inhibited channels become uninhibited, that is why the conditionally expected value of N^o_{n+1} is a monotonically increasing function of τ_n.

In order to obtain the probability of having an event with N^o open channels that occurs at a time, t, after the occurrence of the previous one, we construct a Markov chain in discrete time for the number of channels that open at each event. The state space is $N^o = \{1, 2, \ldots, N\}$, and the transition probabilities are given by

$$P\big(N^o_{n+1} = k/N^o_n = j\big) = \int_o^\infty \mathrm{d}t P\big(N^o_{n+1}(t) = k/N^o_n = j\big) f_{\tau/N^o=j}(t). \quad (5)$$

The stationary measure, $P(N^o = k)$, can then be obtained by solving

$$P(N^o = k) = \sum_{j=1}^{N} P\big(N^o_n = k/N^o_{n-1} = j\big) P(N^o = j), \quad (6)$$

with which the interpuff time marginal distribution can be computed:

$$f_\tau(t) = \sum_{j=1}^{N} f_{\tau/N^o=j}(t) P(N^o = j). \quad (7)$$

2.3. Buffer regulation

The stationary probabilities of equations (6) and (7) allow us to analyze, in a relatively simple way, how the presence of different amounts and types of Ca^{2+} buffers affect the dynamics of puffs. This analysis is relevant because puffs are observed in experiments in which exogenous buffers are used to prevent wave propagation. The Ca^{2+}–buffer interaction can be thought of as a 'leak' term in the $[Ca^{2+}]$ reaction–diffusion equation. Thus, we may expect that, as the buffer concentration is increased, the fluorescence amplitude should decrease. Namely, the added buffer is reducing the free $[Ca^{2+}]$ within the cluster and this should induce the fluorescence to decrease. However, by reducing the value of $[Ca^{2+}]$ the buffer can also interfere with the inhibitory effect of Ca^{2+} on IP_3Rs, allowing more channels in a cluster to open. Therefore, buffers are able to induce two different effects and the final outcome will depend on the amount and kinetics of the buffer that is added. It is important to remark that the inhibitory effect described previously does not apply to experiments that look at the modulation by buffers of the first release event's amplitude. In particular, it does not apply to experiments in which caged IP_3 is photoreleased only at the beginning. It does not explain, for example, the slight amplitude potentiation observed in [4] after the addition of the slow buffer, EGTA. The cluster auto-inhibition is not captured in this last situation as it is in our model. It is not captured either in a situation when paired photolysis flashes are applied with a large temporal separation. All the results presented here must be contrasted with experiments with constant $[IP_3R]$ (as in the experiments of [33]). Observing the effect predicted by our model in experiments, however, is not so easy. Having a larger N_o in the presence of a buffer will not necessarily be reflected into a larger fluorescence due to buffer trapping. Thus, in order to validate this prediction, an algorithm should be applied to estimate the Ca^{2+} current that underlies the image [41].

Table 1. Parameters of the reaction–diffusion equation.

Species	$D\left[\frac{\mu m^2}{s}\right]$	K_d [μM]	$k_{on}\left[\frac{\mu M}{s}\right]$
Fluo (40 μM)	15	3	450
EGTA	200	0.15	5
BAPTA	200	0.16	500
X (immobile buffer 500 μM)	0	18	3

2.3.1. *Estimating the effect of buffers on the release of Ca^{2+} from a cluster of IP_3Rs.*

In order to estimate to what extent exogenous buffers such as BAPTA or EGTA can interfere with the process of Ca^{2+} release from a cluster of IP_3Rs we first study the dynamics of $[Ca^{2+}]$ in the presence of buffers and a constant Ca^{2+} source. We do this with numerical simulations of the set of reaction–diffusion equations describing the dynamics of $[Ca^{2+}]$, an immobile buffer, X, a dye (Fluo 4) and an exogenous buffer (either EGTA or BAPTA) in the presence of a constant 0.5 pA point source of Ca^{2+} located at the origin. The parameters of the simulations are shown in table 1. For Ca^{2+} we use the free diffusion coefficient, $D_{Ca^{2+}} = 220\ \mu m^2\ s^{-1}$, and always the same basal concentration $[Ca^{2+}]_{basal} = 0.04\ \mu M$ given that, in the experiments of [4], both the exogenous buffer and free Ca^{2+} are added so as to keep basal $[Ca^{2+}]$ approximately equal to its value in the absence of the added buffer. We show in figures 2 (*a*) and (*b*) the results of these simulations. In particular, we display in figure 2(*a*) the asymptotic value of $[Ca^{2+}]$ as a function of the distance to the point source in the presence of different amounts of either EGTA or BAPTA. We show in the inset the value of $[Ca^{2+}]$ averaged over a sphere of radius, $r = 10$ nm, around the origin, as a function of the exogenous buffer concentration. We observe that, around the channel's mouth, $[Ca^{2+}]$ decreases by less than 2% with respect to the control situation in the presence of 2500 μM of EGTA while it decreases by ~4.5% in the presence of 100 μM of BAPTA and by ~13% for [BAPTA] = 500 μM. For distances of 60 nm it decreases by less than 20% with respect to the control situation for [EGTA] = 2500 μM, by ~44% in the presence of 100 μM of BAPTA and by ~78% for [BAPTA] = 500 μM. This let us conclude that the free calcium distribution within the cluster region is practically unaffected by the presence of EGTA even at concentrations as large as 2.5 mM. Moderate amounts (~100 μM) of BAPTA, on the other hand, already affect $[Ca^{2+}]$ within the cluster decreasing its value considerably with respect to the control situation. The difference between both behaviors is amplified in the calcium-bound dye concentration, as can be observed in figure 2(*b*) where we show this concentration, $[FluoCa^{2+}]$, as a function of the distance to the source for the same simulations as in figure 2(*a*). The Ca^{2+}-bound dye concentration is a linear (increasing) function of the fluorescence distribution observed in optical experiments [41]. At the channel's mouth, $[FluoCa^{2+}]$ decreases by less than 8% with respect to the

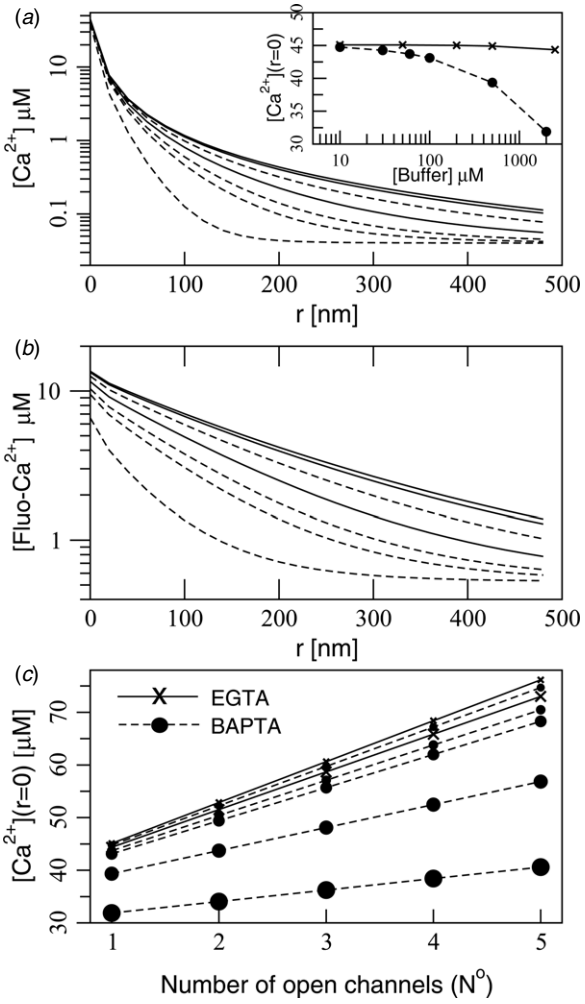

Figure 2. (*a*) $[Ca^{2+}]$ as a function of the distance to the point source in the presence of [EGTA] = 10, 200, 2500 μM (solid lines) and in the presence of [BAPTA] = 10, 60, 100, 500, 2000 μM (dashed lines). The curve that corresponds to the control situation ([EGTA] = [BAPTA] = 0) is indistinguishable from the one with [EGTA] = 10 μM on the scale of this figure. Inset: $[Ca^{2+}]$ at $r = 0$ in the presence of [EGTA] (crosses) and of [BAPTA] (circles), as a function the corresponding exogenous buffer concentration. (*b*) Concentration of Ca^{2+}-bound dye as a function of the distance to the source for the same simulations as in (*a*). (*c*) $[Ca^{2+}]$ at the mouth of an open channel as a function of the total number of open channels in the same cluster. The cytosol includes the presence of [EGTA] = 10, 50, 200, 500, 2500μM (crosses), or [BAPTA] = 10, 30, 60, 100, 500, 2000 μM (solid circles). The size of the symbols is related to the concentration value.

control situation in the presence of 500 μM of EGTA, while it decreases by ∼40% in the presence of 60 μM of BAPTA. For distances of the order of the spatial range of the point spread function of the microscopes with which fluorescence images of Ca^{2+} signals are obtained (∼300 nm), $[FluoCa^{2+}]$ decreases by less than 16%, with respect to the control, in the presence of 500 μM of EGTA and by ∼62% in the presence of 60 μM of BAPTA. Furthermore, the integral of $[FluoCa^{2+}]$ over a sphere of radius 300 nm around the channel's mouth (which gives an estimate of the signal's fluorescence amplitude at the pixel that corresponds to the location of the open channel) changes noticeably in the presence of small amounts of BAPTA. This shows that the differences in the free $[Ca^{2+}]$ distribution within the cluster region in the presence of BAPTA or EGTA should be amplified in the images that are obtained with optical experiments.

Figures 2(*a*) and (*b*) illustrate how the free Ca^{2+} distribution and the corresponding observed Ca^{2+} signals are affected by the presence of different exogenous buffers, provided that the underlying Ca^{2+} current remains always the same. We must note, however, that a change of $[Ca^{2+}]$ within the cluster region with respect to the control situation can alter the kinetics of the channels in the cluster, changing, in turn, the net Ca^{2+} current. The possibility that this occurs depends on the mean separation between IP_3-bound IP_3Rs. There is not a clear picture yet of the intracluster spatial organization [21, 28, 29, 53]. The studies of [28] show that Ca^{2+} puffs can be triggered over a range of IP_3R architectures and that the first channel to become open fails to trigger a puff only at distances larger than 200 nm. This limit agrees with the 'radius of influence' due to CICR estimated in [29] to account for the observations of [52]. In the simple model of [29] all IP_3-bound IP_3Rs within a radius of influence of an open IP_3R become open during a puff. According to the simulations of figure 2(*a*), in the control case this distance corresponds to $[Ca^{2+}] \approx 0.5$ μM. We then observe in figure 2(*a*) that for almost all of the cases studied (the only exception being [BAPTA] = 2 mM, which has not been analyzed experimentally in [4]) $[Ca^{2+}] \geqslant 0.5$ μM at distances ∼100 nm or less from the open source. Given the cluster spatial extent estimated in [53], an inter-IP_3R separation of ∼100 nm seems reasonable for clusters with about five IP_3-bound IP_3Rs. The mean time it takes for an IP_3R with IP_3 bound to bind Ca^{2+} on its activating site, on the other hand, is ∼10 ms at $[Ca^{2+}] \sim 0.5$ μM [34] which is shorter than the typical puff duration (∼100 ms). Thus, considering a mean inter-channel distance of 100 nm, we expect our assumption that any open IP_3R elicits the opening of all other activatable IP_3Rs of the cluster to hold for all the cases studied in figure 2(*a*) with the exception of the one with [BAPTA] = 2 mM. This means that the amounts of BAPTA or EGTA probed in [4] should not alter the CICR coupling between channels of a cluster. The inhibition probability of the IP_3Rs, however, does not necessarily remain the same.

2.3.2. Estimating the effect of buffers on IP_3R inhibition. In order to assess the effect of the exogenous buffers on the IP_3Rs inhibition probability during the time course of a puff, we estimate the value of $[Ca^{2+}]$ at an open channel's mouth when there is a total of N_o open channels in the same cluster as

$$[Ca^{2+}]_s(r = 0) + (N_o - 1)[Ca^{2+}]_s(r = 100 \text{ nm}), \qquad (8)$$

where $[Ca^{2+}]_s(r)$ is the stationary solution in the presence of a single 0.5 pA Ca^{2+} source located at the origin. In this equation we are assuming that each open IP_3R contributes to the free $[Ca^{2+}]$ at the location of any other open IP_3R as if all of them were separated by a distance ∼100 nm. This superposition, on the other hand, is valid as long as the buffers do not become saturated (something that does not happen for the number of open channels that we have considered in this paper). We show in figure 2(*c*) a plot of $[Ca^{2+}]$ at the mouth of one open channel

as a function of the total number of open channels, N_o, in the presence of different amounts of EGTA (open circles) and BAPTA (crosses). We can observe that while $[Ca^{2+}]_s(r = 0)$ practically does not change with respect to the control situation for [EGTA] as large as 2500 μM, it is reduced by 50% in the presence of [BAPTA] = 500 μM, regardless of the number of open channels.

In order to estimate how the inhibition probability of each IP_3R, p_{inh}, changes depending on the intensity of the calcium source (i.e., the number of open channels) and the amount and properties of the exogenous buffers, we need a more detailed description of the IP_3R kinetics than the one used so far. There is still some controversy on which channel kinetic model gives a good description of IP_3Rs [38–40, 42–48, 50, 51] including which are appropriate binding parameters. We avoid the problem of choosing an IP_3R kinetic model by considering a classical Hill equation [49] to give the fraction of IP_3Rs with Ca^{2+} bound to the inhibitory site/s. This fraction can be considered as a good approximation of the probability of inhibition in our model, namely, we assume that p_{inh} and $[Ca^{2+}]$ are related by

$$p_{inh} = \frac{[Ca^{2+}]^n}{K_d^n + [Ca^{2+}]^n}. \quad (9)$$

Combining equations (8) and (9) we obtain $p_{inh}(N^o)$ as needed by our model:

$$p_{inh}(N^o) = \frac{([Ca^{2+}]_s(r = 0) + (N_o - 1)[Ca^{2+}]_s(r = 100\text{ nm}))^n}{K_d^n + ([Ca^{2+}]_s(r = 0) + (N_o - 1)[Ca^{2+}]_s(r = 100\text{ nm}))^n}. \quad (10)$$

In particular, the results of [51] show that this equation describes well the inhibition observed in electrophysiological experiments performed on IP_3Rs of *Xenopus Laevis* oocytes using $n = 4$ and an IP_3-dependent K_d that satisfies $K_d \leqslant 52$ μM (see figure 7(A) of [51]). We show in figure 3(*a*) a plot of p_{inh} as a function of the number of open channels for the particular choice, $K_d = 50$ μM, and $n = 4$. In this figure, p_{inh} is computed using equation (10) with the values of $[Ca^{2+}]$ at $r = 0$ and 100 nm shown in figure 2(*a*) for various amounts of EGTA and BAPTA (see figure caption). Modifying K_d and n we can obtain inhibition curves that vary more or less abruptly with $[Ca^{2+}]$. For example, if we fix $K_d = 1$ μM and $n = 1$ we observe that $p_{inh}(N^o)$ is almost constant and almost independent of the buffer concentration (in the worst case $p_{inh} = 30/31 \approx 70/71$, with each value corresponding to a different buffer). Regardless of the value of K_d, the inhibition probability given by equation (10) will never give well separated curves if the corresponding $[Ca^{2+}]$ versus N^o curves are too close to one another, i.e. very similar calcium profiles give very similar inhibition probability curves. We then conclude that the presence of even very large amounts (2.5 mM) of EGTA do not affect the $[Ca^{2+}]$ and, consequently, the kinetics of the IP_3Rs in the cluster. The local Ca^{2+}-bound dye concentration, which is directly related to the observed fluorescence distribution, is not affected either. Thus, the presence of a slow buffer like EGTA does not alter the dynamics of the cluster as a whole. The presence of

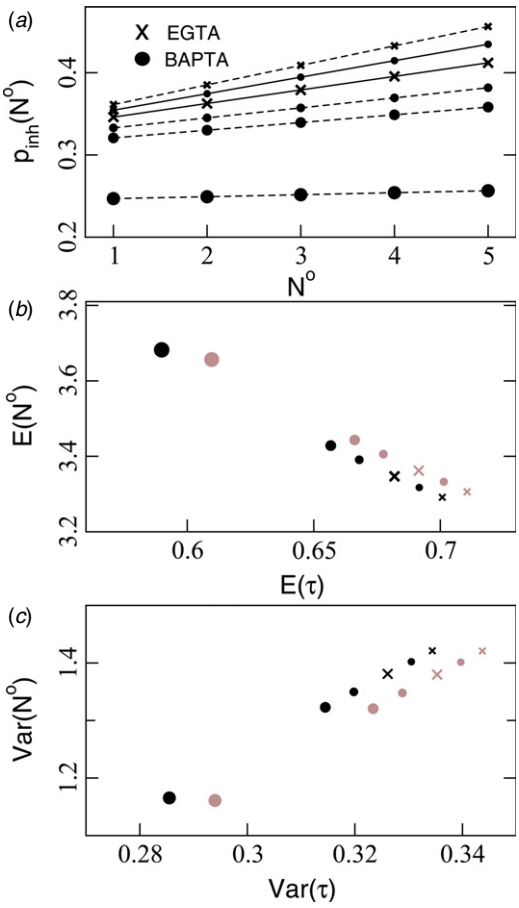

Figure 3. (*a*) IP_3R inhibition probability, p_{inh}, given by equation (10) as a function of the number of open channels in the cluster, N^o. Each curve of this figure was drawn using one of the values of the $[Ca^{2+}]$ at the mouth of the channel shown in figure 2(*c*) which correspond to [EGTA] = 10, 2500 μM (crosses), and [BAPTA] = 10, 60, 100, 500 μM (solid circles). The other parameters used in equation (10) are $K_d = 45$ μM and $n = 10$. For each $p_{inh}(N^o)$ profile, the expected values and variances of N^o and τ are shown in (*b*) and (*c*), respectively, with crosses for EGTA and solid circles for BAPTA. In both cases, larger symbols correspond to larger buffer concentrations, black symbols to $\lambda_1 = 0.5\,s^{-1}$ and grey ones to $\lambda_1 = 0.49\,s^{-1}$. The rest of the parameters used are $\lambda_2 = 1\,s^{-1}$, and $N = 5$.

BAPTA, on the other hand, does reduce significantly the value of $[Ca^{2+}]$, the Ca^{2+}-bound dye concentration and the inhibition probability. This reduction of the signal's amplitude with respect to the control situation, which is larger as the number of open channels increases, cannot be accounted for with a heuristic cluster model that does not consider the effect of the (added) exogenous buffer on the cluster behavior.

2.4. The simple IP_3R-cluster model in the presence of different amounts of buffers

Now we are able to study the cluster model considering the effect of added exogenous buffers. Each 'buffer setting' corresponds to a particular choice of the inhibitory function, $p_{inh}(N^o)$. Given a buffer setting, we study two simple observables: the expected number of channels that participate of a puff, $E(N^o)$, and the mean interpuff time, $E(\tau)$, with

their respective variances. These values, which are easy to determine experimentally, can be derived quite easily from equations (6) and (7). Figure 3(*b*) shows $E(N^o)$ as a function of $E(\tau)$ and figure 3(*c*) the corresponding variances obtained assuming that p_{inh} is the function displayed in figure 3(*a*). The values obtained for [EGTA] = 10, 2500 μM (crosses) are plotted with crosses and those obtained for [BAPTA] = 10, 60, 100, 500 μM are plotted with solid circles. Larger symbols correspond to larger buffer concentrations. In spite of the inhibitory effect, the expected number of channels that participate of a puff increases as the buffer concentration is increased, while the expected interpuff time decreases. This effect is more noticeable for the rapid buffer, BAPTA. For EGTA the expected values do not vary significantly.

The increment of $E(N^o)$ as the concentration of the fast buffer BAPTA increases is of particular interest. It must be noted here that this expected value corresponds to the mean number of open channels over a sequence of events. Namely, with this model we are trying to describe experiments in which [IP_3] and the amount of basal [Ca^{2+}] remains approximately constant during most of the time between subsequent Ca^{2+} release events and where several localized Ca^{2+} signals (puffs) occur at the same IP_3R cluster. Thus, $E(N^o)$ is the expected value for a sequence of events that occur at the same release site. It is somewhat counter-intuitive that $E(N^o)$ increases with increasing BAPTA. Such a fast buffer should decrease the free calcium concentration and, in this way, disrupt CICR between channels. Given the simulations of figure 2 we are assuming that the amounts of BAPTA probed in the subsequent figures are not enough to disrupt CICR within a cluster. The net effect of this fast buffer is then to decrease the number of IP_3Rs that stay inhibited after a puff and, in this way, allow the occurrence of sequences of events that involve more open IP_3Rs as [BAPTA] gets larger. This result is consistent with the simulations of [24] where it was observed that with moderate amounts of BAPTA IP_3R inhibition within a cluster is reduced more drastically than activation. The increment of N_o that we found in our model would be observable in real experiments depending on whether it could be counter-balanced or not by the buffering effect of BAPTA. Namely, if BAPTA traps the released Ca^{2+} ions faster than the dye, most likely the increment of N_o would not result in an increased fluorescence.

In order to show that the results presented here are robust and not the result of a fine tuning of the model parameters we study $E(N^o)$ for an ideal infinitely rapid buffer. In this case, we assume that the Ca^{2+} concentration that an open channel, *i*, senses is only due to the ions that are being released through the same channel, i.e., that the contribution to [Ca^{2+}] from its open neighbors is negligible compared to the value of [Ca^{2+}] due to the ions that go through channel *i*. This situation can hold and still each open channel can induce the opening of its activatable neighbors of the cluster: an increase of 20 nM in [Ca^{2+}] from [Ca^{2+}]$\sim$200 nM can open a channel with high probability while the inhibition probability is not altered by an increase from 40 to 40.02 μM. In this way, it can be assumed that $p_{\text{inh}}(N^o) = p_{\text{inh}}$, independent of the number of open channels, N^o. Under this assumption, it is easy to prove that $E(N^o)$ is a decreasing function of p_{inh} with $E(N^o) = N$ for $p_{\text{inh}} = 0$. Thus, for the limiting case of a constant p_{inh} (i.e., independent of N^o), $E(N^o)$ is a decreasing function of p_{inh} and, therefore, an increasing function of the amount of (fast) exogenous buffer. Other choices of $p_{\text{inh}}(N^o)$, e.g., those of figure 3(*a*), can also lead to expected values, $E(N^o)$, that increase with the buffer concentration.

It is important to remark, that besides the effect we have just described, if an exogenous buffer is added without adding Ca^{2+} to keep its basal concentration constant, the possibly subsequent reduction in basal calcium can also lead to a larger $E(N^o)$. This is also illustrated in figure 3. Namely, the only difference between the results displayed with black and grey symbols in figures 3(*b*) and (*c*) is the value of λ_1 which is slightly smaller for the grey symbols than for the black ones. The parameter, λ_1, is proportional to the amount of Ca^{2+} in the system because it represents the probability per unit time that one IP_3R becomes open in the presence of basal Ca^{2+}. Given that equally sized symbols correspond to the same buffer concentration we observe in figure 3(*b*) that $E(N^o)$ increases when basal Ca^{2+} (or, equivalently, λ_1) decreases. The difference between the effects of decreasing basal Ca^{2+} or increasing the exogenous buffer concentration is observable in the expected interpuff time, $E(\tau)$. Namely, as it may be observed in figure 3(*b*), $E(\tau)$ decreases with increasing buffer concentration while it increases with decreasing basal Ca^{2+}. In summary, a decrease in basal Ca^{2+}[33] and/or an increment in buffer concentration increase the mean puff size computed from a sequence of Ca^{2+} release events that occur at the same site. The mean interpuff time, on the other hand, increases with decreasing basal Ca^{2+} and decreases with increasing buffer concentration. This different effect could in principle be checked in experiments.

Finally, in figure 3(*c*) we show the variances of N^o and τ for each buffer scenario. Interestingly both variances decrease when the amount of buffer is increased while basal Ca^{2+} is kept fixed (black symbols). A small change in the basal Ca^{2+} concentration, on the other hand, produces a large change in $\text{Var}(\tau)$, while $\text{Var}(N^o)$ does not undergo significant changes. This effect of basal Ca^{2+} on the variance of event sizes resembles the observations of [55] where Ca^{2+}-mediated intracluster coupling was key to go from a long-tailed to a Gaussian-like event size distribution.

3. Conclusions

Cytosolic Ca^{2+} induces different physiological responses depending on the spatio-temporal dynamics of its concentration. The presence of *buffers*, substances that bind and unbind Ca^{2+}, provides a mechanism by which the cell can modulate this spatio-temporal dynamics. In particular, the expression of different types of buffers (with different concentrations, reaction and diffusion rates) lead to different Ca^{2+} behaviors. In this paper we have introduced a model that is simple enough so that it is amenable to analytic computations but still gives meaningful information on the ways in which buffers affect the dynamics of sequences of Ca^{2+} puffs.

In [4] the effect of the exogenous buffers, EGTA and BAPTA, on the dynamics of Ca^{2+} that followed a single

IP_3 release was studied. These studies were done in *Xenopus Laevis* oocytes and were subsequently extended to two buffers, Parvalbumin and Calretinin, expressed endogenously in the same cell type [3]. In both types of experiments the authors found that the slow buffers, EGTA or Parvalbumin, disrupt CICR between IP_3R clusters leading to localized signals whereas the fast ones, BAPTA or Calretinin, lead to global signals that are spatially diffuse and decay slowly. The experiments of [3, 4] differ in two aspects with respect to the situation analyzed in the present paper. In [3, 4] IP_3 is photoreleased only initially and the interaction between different IP_3R clusters is then studied. Here we analyze the effect of Ca^{2+} puffs on subsequent release events that occur at the same site in the presence of a constant amount of IP_3, a situation that can be attained with a continuous UV illumination as done in [33]. The observations of [4] (e.g. the increment in the first event amplitude when [EGTA] is slightly increased or the continuous Ca^{2+} release in the presence of large amounts of [BAPTA]) are hard to interpret because of their non-stationarity. Our results show that even in the simpler, stationary situation, buffers produce non-trivial effects on the dynamics of puffs such as the increment in the mean number of open channels in the presence of low concentrations of BAPTA. In the stationary regime, there is a competition between basal Ca^{2+} that promotes event generation and inhibition that prevents it. In this regime buffers basically modulate the dynamics of clusters by modifying the inhibition probability of the individual channels. Our model relies on the assumption that the opening probability of the channels remains unaffected by the presence of the buffers. We believe that this toy model captures the essence of sequences of puffs that occur at the same release site.

3.1. An interpretation for the 'buffer effect'

The effect of fast buffers on the cluster dynamics via a reduction of IP_3R inhibition has been observed in the simulations of [24, 26] for clusters where activatable IP_3Rs are close enough to one another. For clusters where the mean inter-IP_3R distance is relatively large, the dominant effect of the addition of fast buffers observed in [24, 26] is to reduce activation. We must note that the quantity that is analyzed in [24, 26] is different from the one we look at with our model. Namely, in [24, 26] the cluster 'open probability', P_o, is computed. If this open probability is computed as in the case of a single IP_3R(i.e., the ratio between the mean time during which there is Ca^{2+} release with respect to the total observation time), then it carries no information on the number of IP_3Rs involved (other than the effect that this number has on the times that are used to compute P_o). In our model the duration of the Ca^{2+} release event is not considered but we do draw information on both the number of IP_3Rs that open during the event and on the interpuff time separately.

According to our model, the mean puff size can also increase when the basal Ca^{2+} concentration is decreased. Contrary to what happens with buffers, this is accompanied by (and is a consequence of) the enlargement of the interpuff time that occurs when there is less Ca^{2+} available to start a release event. In this way, it takes a longer time to open the IP_3R that triggers the event, there are fewer IP_3Rs that are still inhibited when this happens and the event has a larger amplitude. The different effects that adding a fast buffer or decreasing basal Ca^{2+} have on sequences of puffs could be checked in experiments in which IP_3 uniformly delivered in time as done in [33].

The situation with a constant rate of IP_3 production is encountered in many physiological conditions when this production is induced by the presence of an external stimulus during a prolonged period of time. As a response to the resulting increment in cytosolic [IP_3] cells can produce global Ca^{2+} elevations (spikes) that repeat themselves with an apparent periodicity. It is believed that information is encoded in the frequency of these oscillations [1]. The analysis of the interspike times has led to the conclusion that these oscillations are far from being regular: interspike times, T, are highly variable with a standard deviation, σ_T, of the same order of magnitude as their mean, $\langle T\rangle$ [31, 32]. Various experimental observations show that the standard deviation and the mean of the interspike time are linearly related with a slope that is smaller than 1, a condition that guarantees that spike trains can transmit information [31]. In spite of the large variability of the interspike time it is shown in [31] that the σ_T versus $\langle T\rangle$ relationship is robust against changes of many parameters, among them, buffers and that the value of the slope is determined by a global inhibitory effect. We do see a similar behavior in our case. Namely, inhibition in our model is global (there is a fixed recovery time, $1/\lambda_2$, for all IP_3Rs) and the mean and deviation of the interpuff time decrease simultaneously with the addition of a fast buffer such as BAPTA (while keeping basal Ca^{2+} fixed) or when basal Ca^{2+} is decreased. For signaling purposes, not only the interpuff time matters but also how the total amount of free Ca^{2+} that is present in the system changes with the stimulus. We can use our model to infer how changes in response to a constant stimulus would vary in the presence of certain perturbations, such as the addition of a fast buffer, by looking at how interpuff times and puff sizes vary. In particular, the average amount of Ca^{2+} released during an observation time, $T_{\rm obs}$, is proportional to $\frac{1}{T_{\rm obs}}\int_0^{T_{\rm obs}} dt \sum_i N_i^o \delta(t - \sum_{k=1,\dots,i}\tau_k)$, where N_i^o and τ_i are the sequences of values that the variables, N^o and τ, take on during the observation time. We can estimate this quantity as $\langle N^o\rangle T_{\rm obs}/\langle\tau\rangle$. Thus, if basal Ca^{2+} remains fixed and a fast buffer is added we expect the amount of Ca^{2+} that is released in the system to be increased. The amount of free Ca^{2+}, however, could remain constant given that the fast buffer would trap part of the released Ca^{2+}. Therefore, changes in free Ca^{2+} in response to a constant stimulus could remain invariant in the presence of a fast buffer. Knowing the final outcome, however, would depend on the balance between the increase in Ca^{2+} release and the reduction of free Ca^{2+} that a fast buffer produces. An increment in basal Ca^{2+}, on the other hand, could lead to an invariant amount of Ca^{2+} released given that both $\langle N^o\rangle$ and $\langle\tau\rangle$ would decrease in such a case. This discussion shows that even if variations in the amount of buffer or in basal Ca^{2+} produce variations in $\langle N^o\rangle$ and $\langle\tau\rangle$ these variations are such that the amount by which the free [Ca^{2+}] changes in response to a constant stimulus could remain invariant. Such

a feature could be relevant for the information transmission capability of the signals. We remark again that we are not looking at the interspike but at the interpuff time interval of puffs that occur at the same release site. In any case, as stated in [31], having a good model of the interpuff time interval inferred out of observations *in vivo* would lead to realistic models of Ca^{2+} signaling pathways without the need to rely on electrophysiological experiments that cannot be done in intact cells.

References

[1] Berridge M J, Bootman M D and Lipp P 1998 Calcium—a life and death signal *Nature* **395** 645–8

[2] Iino M 1990 Biphasic calcium dependence of inositol trisphosphate induced calcium release in smooth muscle cells of the guinea pig Taenia caeci *J. Gen. Physiol.* **95** 1103–22

[3] Dargan S, Schwaller B and Parker I 2004 Spatiotemporal patterning of IP_3 mediated Ca^{2+} signals in Xenopus oocytes by Ca^{2+}binding proteins *J. Physiol.* **556** 447–61

[4] Dargan S and Parker I 2004 Buffer kinetics shape the spatiotemporal patterns of IP_3-evoked Ca^{2+} signals *J. Physiol.* **553** 775–88

[5] Yao Y, Choi J and Parker I 1995 Quantal puffs of intracellular Ca^{2+} evoked by inositol trisphosphate in Xenopus oocytes *J. Physiol.* **482** 533–53

[6] Sun X, Callamaras N, Marchant J S and Parker I 1998 A continuum of $InsP_3$-mediated elementary Ca^{2+} signalling events in Xenopus oocytes *J. Physiol.* **509** 67–80

[7] Ponce Dawson S, Keizer J and Pearson J E 1999 Fire-diffuse-fire model of dynamics of intracellular calcium waves *Proc. Natl Acad. Sci. USA* **96** 6060–3

[8] Keizer J and Smith G D 1998 Spark-to-wave transition: saltatory transmission of calcium waves in cardiac myocytes *Biophys. Chem.* **72** 87–100

[9] Timofeeva Y and Coombes S 2004 Directed percolation in a two-dimensional stochastic fire-diffuse-fire model *Phys. Rev.* E **70** 062901

[10] Coombes S and Timofeeva Y 2003 Sparks and waves in a stochastic fire-diffuse-fire model of Ca^{2+} release *Phys. Rev.* E **68** 021915

[11] Calabrese A, Fraiman D, Zysman D and Ponce Dawson S 2010 A stochastic fire-diffuse-fire model with realistic cluster dynamics *Phys. Rev.* E **82** 031910

[12] Shuai J W and Jung P 2002 Stochastic properties of Ca^{2+} release of inositol 1,4,5-trisphosphate receptor clusters *Biophys. J.* **83** 87–97

[13] DeRemigio H and Smith G D 2005 The dynamics of stochastic attrition viewed as an absorption time on a terminating Markov chain *Cell Calcium* **38** 73–86

[14] Diambra L and Guisoni N 2005 Modeling stochastic Ca^{2+} release from a cluster of IP_3-sensitive receptors *Cell Calcium* **37** 321–32

[15] Ullah G and Jung P 2006 Modeling the statistics of elementary calcium release events *Biophys. J.* **90** 3485–95

[16] Shuai J and Jung P 2003 Sub-threshold Ca^{2+}waves *New J. Phys.* **5** 132

[17] Thul R and Falcke M 2004 Release currents of IP(3) receptor channel clusters and concentration profiles *Biophys. J.* **86** 2660–73

[18] Bar M, Falcke M, Levine H and Tsimring L S 2000 Discrete stochastic modeling of calcium channel dynamics *Phys. Rev. Lett.* **84** 5664–7

[19] Falcke M, Tsimring L and Levine H 2000 Stochastic spreading of intracellular Ca2+ release *Phys. Rev.* E **62** 2636–43

[20] Swillens S, Champeil P, Combettes L and Dupont G 2008 Stochastic simulation of a single inositol 1,4,5-trisphosphate-sensitive Ca^{2+} channel reveals repetitive openings during 'blip-like' Ca^{2+} transients *Cell Calcium* **23** 291–302

[21] Swillens S, Dupont G, Combettes L and Champeil P 1999 From calcium blips to calcium puffs: theoretical analysis of the requirements for interchannel communication *Proc. Natl Acad. Sci. USA* **96** 13750–5

[22] Rüdiger S, Shuai J W, Huisinga W, Nagaiah C, Warnecke G, Parker I and Falcke M 2007 Hybrid stochastic and deterministic simulations of calcium blips *Biophys. J.* **93** 1847–57

[23] Solovey G, Fraiman D, Pando B and Ponce Dawson S 2008 Simplified model of cytosolic Ca^{2+} dynamics in the presence of one or several clusters of Ca^{2+}-release channels *Phys. Rev.* E **78** 041915

[24] Rüdiger S, Nagaiah Ch, Warnecke G and Shuai J W 2010 Calcium domains around single and clustered IP_3 receptors and their modulation by buffers *Biophys. J.* **99** 3–12

[25] Shuai J, Pearson J E and Parker I 2008 Modeling Ca^{2+} feedback on a single inositol 1,4,5-trisphosphate receptor and its modulation by Ca^{2+} buffers *Biophys. J.* **95** 3738–52

[26] Rudiger S, Shuai J W and Sokolov I M 2010 Law of mass action, detailed balance, and the modeling of calcium puffs *Phys. Rev. Lett.* **105** 048103

[27] Solovey G, Fraiman D and Ponce Dawson S 2011 Mean field strategies induce unrealistic nonlinearities in calcium puffs *Front. Physiol.* **2** 00046

[28] Diambra L and Marchant J S 2011 Inositol (1,4,5)-trisphosphate receptor microarchitecture shapes Ca^{2+} puff kinetics *Biophys. J.* **100** 822–31

[29] Solovey G and Ponce Dawson S 2010 Intra-cluster percolation of calcium signals *PLoS ONE* **2** e8997

[30] Solovey G and Ponce Dawson S 2010 Observable effects of Ca^{2+} buffers on local Ca^{2+} signals *Phil. Trans. R. Soc.* A **368** 5597–603

[31] Thurley K and Falcke M 2011 Derivation of Ca^{2+} signals from puff properties reveals that pathway function is robust against cell variability but sensitive for control *Proc. Natl Acad. Sci. USA* **108** 427–32

[32] Skupin A, Kettenmann H, Winkler U, Wartenberg M, Sauer H, Tovey S, Taylor C and Falcke M 2008 How does intracellular Ca21 oscillate: by chance or by the clock? *Biophys. J.* **94** 2404–11

[33] Fraiman D, Pando B, Dargan S, Parker I and Ponce Dawson S 2006 Analysis of Puff dynamics in oocytes: interdependence of puff amplitude and inter-puff interval *Biophys. J.* **90** 3897–907

[34] Fraiman D and Ponce Dawson S 2004 A model of the IP_3 receptor with a luminal calcium binding site: stochastic simulations and analysis *Cell Calcium* **35** 403–13

[35] Thul R and Falcke M 2004 Release currents of IP_3 receptor channel clusters and concentration profiles *Biophys. J.* **86** 2660–73

[36] Solovey G, Fraiman D, Pando B and Ponce Dawson S 2008 Simplified model of cytosolic Ca^{2+} dynamics in the presence of one or several clusters of Ca^{2+} release channels *Phys. Rev.* E **78** 41915–29

[37] Taufiq-Ur-Rahman , Skupin A, Falcke M and Taylor C 2009 Clustering of $InsP_3$ receptors by $InsP_3$ retunes their regulation by $InsP_3$ and Ca^{2+} *Nature* **458** 655–9

[38] Swillens S, Combettes L and Champeil P 1994 Transient inositol 1,4,5-trisphosphate-induced Ca^{2+} release: a model based on regulatory Ca^{2+} binding sites along the permeation pathway *Proc. Natl Acad. Sci. USA* **91** 10074–8

[39] Fraiman D and Ponce Dawson S 2004 A model of the IP_3 receptor with a luminal calcium binding site: stochastic simulations and analysis *Cell Calcium* **35** 403–13

[40] De Young G W and Keizer J 1992 A single-pool inositol 1,4,5-triphosphate-receptor-based model for agonist-stimulated oscillations in Ca^{2+} concentration *Proc. Natl Acad. Sci. USA* **89** 9895–9

[41] Ventura A C, Bruno L, Demuro A, Parker I and Ponce Dawson S 2005 A model-independent algorithm to derive Ca^{2+} fluxes underlying local cytosolic Ca^{2+} transients *Biophys. J.* **88** 2403–21

[42] Bezprozvanny I 1994 Theoretical analysis of calcium wave propagation based on inositol (1,4,5)-trisphosphate (IP_3) receptor functional properties *Cell Calcium* **16** 151–66

[43] Taylor C W 1994 Inositol triphosphate receptors: Ca^{2+} modulated intracellular Ca^{2+} channels *Biochim. Biophys. Acta* **1436** 19–33

[44] Taylor C W 1998 Inositol trisphosphate receptors: Ca^{2+}-modulated intracellular Ca^{2+} channels *Biochim. Biophys. Acta* **1436** 19–33

[45] Shinohara T *et al* 2011 Mechanistic basis of bell-shaped dependence of inositol 1,4,5-trisphosphate receptor gating on cytosolic calcium *Proc. Natl Acad. Sci. USA* **108** 15486–91

[46] Siekmann I, Wagner L E, Yule D, Crampin E J and Sneyd J 2012 A kinetic model for type I and II IP_3R accounting for mode changes *Biophys. J.* **103** 658–68

[47] Ullah G, Mak D O D and Pearson J E 2012 A data-driven model of a modal gated ion channel: the inositol 1,4,5-trisphosphate receptor in insect Sf9 cells *J. Gen. Physiol.* **140** 159–73

[48] Shuai J W, Yang D P and Pearson J E 2009 An investigation of models of the IP_3R channel in Xenopus oocyte *Chaos* **19** 037105

[49] Weiss J N 1997 The Hill equation revisited: uses and misuses *FASEB J.* **11** 835–41

[50] Hitur K and Linne M-L 2013 Comparison of models for IP_3 receptor kinetics using stochastic simulations *PLoS ONE* **8** e59618

[51] Foskett J K, White C, Cheung K-H and Mak D-O D 2007 Inositol trisphosphate receptor Ca^{2+} release channels *Physiol. Rev.* **87** 593–658

[52] Smith I F and Parker I 2009 Imaging the quantal substructure of single IP_3R channel activity during Ca^{2+} puffs in intact mammalian cells *Proc. Natl Acad. Sci USA* **106** 6404–9

[53] Bruno L, Solovey G, Ventura A C, Dargan S and Ponce Dawson S 2010 *Cell Calcium* **47** 273–86

[54] Zeller S, Rüdiger S, Engel H, Sneyd J, Warnecke G, Parker I and Falcke M 2009 Modeling of the modulation by buffers of Ca^{2+} release through clusters of IP_3 receptors *Biophys. J.* **97** 992–1002

[55] Lopez L, Piegari E, Sigaut L and Ponce Dawson S 2012 Intracellular calcium signals display an avalanche-like behavior over multiple lengthscales *Front. Physiol.* **3** 350

QUERIES

Page 10

Q1

Author: Please check the details for any journal references that do not have a blue link as they may contain some incorrect information. Pale purple links are used for references to arXiv e-prints.

Q2

Author: Please provide initials of the first author (Taufiq-Ur-Rahman) in reference [37].

Page 11

Q3

Author: References [43] and [44] are identical. Please delete one of them and renumber the subsequent references in the list and the text accordingly or replace one of them with the new one.

Q4

Author: Please check whether the years in references [46, 55] are okay as included.

Q5

Author: Reference [54] is not cited in the text. Please cite the same in the text as appropriate or else delete from the list.